PADOVA UNIVERSITY PRESS

Dolomites Research Notes on Approximation

Volume 14 · 2021 · Pages 27–32

Convergence rate in terms of the continuous SSIM (cSSIM) index in RBF interpolation

Francesco Marchetti[a]

Communicated by L. Bos

Abstract

The Structural Similarity index (SSIM) is a very popular tool for the evaluation of the similarity between two images. In this work, we extend it by introducing the continuous SSIM (cSSIM) index. Then, focusing on Radial Basis Function (RBF) interpolation, we provide theoretical results concerning the convergence rate of a RBF interpolant in terms of the cSSIM index. The theoretical findings are then confirmed by numerical experiments.

1 Introduction

The Structural Similarity index (SSIM) [10] is widely-employed in assessing the similarity between two images. Indeed, in several studies, it proved to perform better than other standard metrics, such as the mean-squared error, in evaluating the perceived quality of image reconstruction methods. Therefore, in recent years such an index has been proposed and adapted to different frameworks, as in e.g. [8, 7], and much work has been devoted to the analysis of its mathematical properties and to the study of related metrics [1]. Moreover, SSIM-based loss functions have been considered in the field of supervised machine learning [12].

Due to its increasing popularity, it has been also considered in the context of 2D function approximation, since the target function to be recovered may be interpreted as an image in many applications [3, 5]. However, detailed analyses of the asymptotic behavior of the SSIM index in interpolation processes are still lacking and have never been taken into consideration.

In this work, we consider the SSIM index in the framework of Radial Basis Function (RBF) interpolation, where the interpolant is built upon (strictly) positive definite radial kernels; we refer to [6, 11] for a complete discussion.

After introducing the continuous SSIM (cSSIM) index, which is directly derived from the standard SSIM score, we investigate the convergence of an RBF interpolant towards the related underlying function in terms of the cSSIM index.

The results obtained in Section 3, which show that the rate of convergence is directly linked to the regularity of the kernel, are then confirmed by numerical tests carried out in Section 4.

2 RBF interpolation

Let $\Omega \subseteq \mathbb{R}^n$ $n \geq 1$ be bounded and let $\mathcal{X} = \{\boldsymbol{x}_i,\ i = 1,\dots,N\} \subset \Omega$ be a set of distinct nodes. Let $\mathcal{F} = \{f_i = f(\boldsymbol{x}_i),\ i = 1,\dots,N\}$ be the set of function values associated to $\mathcal{X}$, which is obtained by sampling some (unknown) function $f : \Omega \longrightarrow \mathbb{R}$. The scattered data interpolation problem consists in approximating f by means of a function $r : \Omega \longrightarrow \mathbb{R}$ which satisfies the interpolating conditions

$$r(\boldsymbol{x}_i) = f_i, \quad i = 1,\dots,N. \tag{1}$$

Here, we look for $r \in \operatorname{span}\{\kappa(\cdot,\boldsymbol{x}_i),\ \boldsymbol{x}_i \in \mathcal{X}\}$, where $\kappa : \Omega \times \Omega \longrightarrow \mathbb{R}$ is a strictly positive definite, radial and symmetric kernel. In this case, the interpolation problem (1) admits a unique solution and the resulting kernel-based interpolant takes the form

$$r(\boldsymbol{x}) = \sum_{i=1}^{N} c_i \kappa(\boldsymbol{x},\boldsymbol{x}_i), \quad \boldsymbol{x} \in \Omega.$$

More precisely, the vector of coefficients $\boldsymbol{c} = (c_1,\dots,c_N)^\intercal$ is obtained by solving the linear system $K\boldsymbol{c} = \boldsymbol{f}$, where $K \in \mathbb{R}^{N\times N}$, $K_{ij} = \kappa(\boldsymbol{x}_i,\boldsymbol{x}_j)$, $i,j = 1,\dots,N$ is the so-called *kernel matrix* and $\boldsymbol{f} = (f_1,\dots,f_N)^\intercal$ is the vector of function values.

We recall that, since κ is radial, there exists a univariate function $\varphi : [0,\infty) \longrightarrow \mathbb{R}$ such that

$$\kappa(\boldsymbol{x},\boldsymbol{y}) = \varphi(\|\boldsymbol{x}-\boldsymbol{y}\|_2) = \varphi(r),$$

where $r = \|\boldsymbol{x}-\boldsymbol{y}\|_2$ and $\|\cdot\|_2$ is the Euclidean norm on $\mathbb{R}^n$.

[a]Department of Mathematics "Tullio Levi-Civita", University of Padova, Italy

Furthermore, we associate to κ a Reproducing Kernel Hilbert Space (RKHS) $\mathcal{N}_\kappa(\Omega)$, also called the *native space*, which is defined as the completion of the pre-Hilbert space

$$\mathcal{H}_\kappa(\Omega) = \text{span}\{\kappa(\cdot, \boldsymbol{x}),\ \boldsymbol{x} \in \Omega\},$$

equipped with the bilinear form $(\cdot,\cdot)_{\mathcal{H}_\kappa(\Omega)}$, with respect to the norm $||\cdot||_{\mathcal{H}_\kappa(\Omega)}$.

The accuracy of the interpolation procedure can be expressed in terms of the so-called *fill distance*, which is defined as

$$h = h_{\mathcal{X},\Omega} = \sup_{\boldsymbol{x}\in\Omega} \min_{\boldsymbol{x}_i\in\mathcal{X}} \|\boldsymbol{x} - \boldsymbol{x}_i\|_2.$$

Indeed, we have the following result.

Theorem 2.1 ([6, Theorem 14.5, p. 121]). *Let $\Omega \subseteq \mathbb{R}^n$ be bounded and suppose that it satisfies an interior cone condition. Moreover, let $\kappa \in C^{2k}(\Omega \times \Omega)$ be a strictly positive definite kernel. Then, there exist positive constants h_0 and C, independent of $\boldsymbol{x}$, f and κ, such that*

$$|f(\boldsymbol{x}) - r(\boldsymbol{x})| \le C h_{\mathcal{X},\Omega}^k \sqrt{C_\kappa(\boldsymbol{x})} \|f\|_{\mathcal{N}_\kappa(\Omega)}, \tag{2}$$

provided $h_{\mathcal{X},\Omega} \le h_0$ and $f \in \mathcal{N}_\kappa(\Omega)$, where

$$C_\kappa(\boldsymbol{x}) = \max_{|\boldsymbol{\beta}|=2k} \left(\max_{\boldsymbol{w},\boldsymbol{z}\in\Omega\cap B\left(\boldsymbol{x}, c_2 h_{\mathcal{X},\Omega}\right)} \left| D_2^{\boldsymbol{\beta}} \kappa(\boldsymbol{w},\boldsymbol{z}) \right| \right),$$

with $B\left(\boldsymbol{x}, c_2 h_{\mathcal{X},\Omega}\right)$ denoting the ball of radius $c_2 h_{\mathcal{X},\Omega}$ centred at $\boldsymbol{x}$, where c_2 is derived from [6, Theorem 14.4, p. 120].

Remark 1. Referring to (2) and denoting the uniform error as $E_{f,r} := \sup_{x\in\Omega} |f(x) - r(x)|$, for any $\boldsymbol{x} \in \Omega$ we can express the interpolation error as

$$r(\boldsymbol{x}) = f(\boldsymbol{x}) + u(E_{f,r})$$

where $u(E_{f,r}) = \mathcal{O}(E_{f,r})$ as $E_{f,r} \to 0$ and thus, since $E_{f,r} = \mathcal{O}(h^k)$ as $h \to 0$,

$$r(\boldsymbol{x}) = f(\boldsymbol{x}) + \bar{u}(h)$$

where $\bar{u}(h) = \mathcal{O}(h^k)$ as $h \to 0$. This formulation will be useful in our analysis.

We point out that the error bound in Theorem 2.1 can be refined for specific kernels. For example, considering the C^k-Wendland kernel or the C^k-Matérn kernel, which are defined e.g. in [11, Definition 9.11, p. 128] and [6, Section 4.4, p. 41] respectively, we have that (see [6, Example 15.4 & Example 15.5, p. 126])

$$|f(\boldsymbol{x}) - r(\boldsymbol{x})| \le C h_{\mathcal{X},\Omega}^{(k+1)/2} \|f\|_{\mathcal{N}_\kappa(\Omega)}, \tag{3}$$

where C is a positive constant. Moreover, specific error bounds for discontinuous kernels have been derived in [4].

3 Convergence in terms of cSSIM index

3.1 Extending the SSIM index

Let $X, Y \in \mathbb{R}_{\ge 0}^{p\times q}$, $p, q \in \mathbb{N}$ be positive-valued matrices representing two images. We consider the SSIM index defined as in [10]

$$\text{SSIM}(X,Y) = \frac{2\mu_X\mu_Y + c_1}{\mu_X^2 + \mu_Y^2 + c_1} \cdot \frac{2\sigma_{X,Y} + c_2}{\sigma_X^2 + \sigma_Y^2 + c_2}, \quad c_1, c_2 > 0, \tag{4}$$

where μ_X, μ_Y are the sample mean of X and Y respectively, while σ_X^2, σ_Y^2 and $\sigma_{X,Y}$ are the sample variances and covariance.

Instead of directly considering the whole images, we point out that the SSIM index is usually obtained by computing (4) on many local windows, then pooling the resulting indices by taking, for example, the mean value. Moreover, the constants c_1, c_2 have been introduced for stability purposes and they are chosen to be *small* positive numbers.

It can be proved that $-1 < \text{SSIM}(X,Y) \le 1$, with $\text{SSIM}(X,Y) = 1$ if and only if $X = Y$. Furthermore, we observe that both $\text{SSIM}(X,Y)$ and the related dissimilarity measure $\text{DSSIM}(X,Y) := 1 - \text{SSIM}(X,Y)$ are not valid metrics, though various SSIM-based distances can be derived; we refer to [2] for a detailed discussion.

Here, we give an extension of (4) for real positive-valued functions. More precisely, letting $f, g : \Omega \longrightarrow \mathbb{R}_{\ge 0}$, $f, g \in L_2(\Omega)$, we consider the expressions

$$\mu_f = \tfrac{1}{\text{meas}(\Omega)} \int_\Omega f \, \mathrm{d}\boldsymbol{x},$$

$$\sigma_{f,g} = \tfrac{1}{\text{meas}(\Omega)} \int_\Omega (f - \mu_f)(g - \mu_g) \, \mathrm{d}\boldsymbol{x},$$

$$\sigma_f^2 = \sigma_{f,f},$$

where $\text{meas}(\Omega)$ is the standard Lebesgue measure of the set Ω. Then, we define the cSSIM index between f and g as

$$\text{cSSIM}(f,g) := \frac{2\mu_f\mu_g + c_1}{\mu_f^2 + \mu_g^2 + c_1} \cdot \frac{2\sigma_{f,g} + c_2}{\sigma_f^2 + \sigma_g^2 + c_2}, \quad c_1, c_2 > 0. \tag{5}$$

We observe that the cSSIM index is indeed a *continuous* extension of the original SSIM, since important properties such as $-1 < \text{cSSIM}(f,g) \le 1$ and $\text{cSSIM}(f,g) = 1$ if and only if $f = g$ a.e. still hold.

Moreover, even if in Section 4 we focus on the case $n = 2$, the cSSIM index may be considered in any dimension $n \in \mathbb{N}$, $n \ge 1$.

3.2 Convergence analysis

In what follows, we investigate the asymptotic behavior of the cSSIM index in the context of RBF interpolation. First, we need the following lemma.

Lemma 1. Let $f, g : \Omega \longrightarrow \mathbb{R}_{\geq 0}$, $f, g \in L_1(\Omega)$ and let $E_{f,g} = \sup_{x\in\Omega} |f(x) - g(x)|$. We have

$$\mu_g = \mu_f + \nu(E_{f,g}).$$

with $\nu(E_{f,g}) = \mathcal{O}(E_{f,g})$ as $E_{f,g} \to 0$.

Proof. As also pointed out in [9], since

$$\left| \int_\Omega f \, \mathrm{d}\boldsymbol{x} - \int_\Omega g \, \mathrm{d}\boldsymbol{x} \right| \leq \mathrm{meas}(\Omega) \sup_{\boldsymbol{x}\in\Omega} |f(\boldsymbol{x}) - g(\boldsymbol{x})|,$$

we have

$$\int_\Omega g \, \mathrm{d}\boldsymbol{x} = \int_\Omega f \, \mathrm{d}\boldsymbol{x} + \mathcal{O}(E_{f,g}).$$

□

Therefore, we obtain the following results. We point out the cSSIM approaches the value of 1 in case of convergence, since it is a similarity index.

Theorem 3.1. *Let $\Omega \subseteq \mathbb{R}^n$ be bounded and let $f : \Omega \longrightarrow \mathbb{R}_{\geq 0}$, $f \in L_2(\Omega)$. Moreover, let κ be a strictly positive definite kernel on $\Omega \times \Omega$ and let r be the κ-based interpolant of f at $\mathcal{X}$ as in (1). Then, letting $E_{f,r} = \sup_{x\in\Omega} |f(x) - r(x)|$, we have that*

$$\mathrm{cSSIM}(f, r) = \frac{1}{1 + \mathcal{O}(E_{f,r}^2)} \quad \text{as } E_{f,r} \to 0.$$

Proof. In the following, we denote $E_{f,r} = E$. Recalling that $\sigma_{f,r} = \mu_{fr} - \mu_f \mu_r$ and in view of Lemma 1 and Remark 1, we get

$$\begin{aligned} \sigma_{f,r} &= \frac{1}{\mathrm{meas}(\Omega)} \int_\Omega f(f + u(E)) \, \mathrm{d}\boldsymbol{x} - \mu_f(\mu_f + \nu(E)) \\ &= \mu_{f^2} - \mu_f^2 + (u(E) - \nu(E))\mu_f \end{aligned}$$

and

$$\begin{aligned} \sigma_r^2 &= \frac{1}{\mathrm{meas}(\Omega)} \int_\Omega (f + u(E))^2 \, \mathrm{d}\boldsymbol{x} - (\mu_f + \nu(E))^2 \\ &= \mu_{f^2} - \mu_f^2 + 2(u(E) - \nu(E))\mu_f + u^2(E) - \nu^2(E). \end{aligned}$$

Therefore, by substituting in the definition (5) with $w(E) := u(E)^2 - \nu(E)^2$ we obtain

$$\begin{aligned} \mathrm{cSSIM}(f, r) &= \frac{2\mu_f(\mu_f + \nu(E)) + c_1}{\mu_f^2 + (\mu_f + \nu(E))^2 + c_1} \cdot \frac{2\sigma_f^2 + 2(u(E) - \nu(E))\mu_f + c_2}{2\sigma_f^2 + 2(u(E) - \nu(E))\mu_f + c_2 + w(E)} \\ &= \frac{2\mu_f^2 + 2\nu(E)\mu_f + c_1}{2\mu_f^2 + 2\nu(E)\mu_f + c_1 + \nu^2(E)} \cdot \frac{2\sigma_f^2 + 2(u(E) - \nu(E))\mu_f + c_2}{2\sigma_f^2 + 2(u(E) - \nu(E))\mu_f + c_2 + w(E)} \\ &= \frac{1}{1 + t_1(E)} \cdot \frac{1}{1 + t_2(E)} = \frac{1}{1 + t_1(E) + t_2(E) + t_1(E)t_2(E)}, \end{aligned}$$

where $t_1(E) := \nu^2(E)/(2\mu_f^2 + 2\nu(E)\mu_f + c_1)$ and $t_2(E) := w(E)/(2\sigma_f^2 + 2(u(E) - \nu(E))\mu_f + c_2)$. Finally, we observe that both $t_1(E)$ and $t_2(E)$ are $\mathcal{O}(E^2)$ as $E \to 0$, thus

$$t_1(E) + t_2(E) + t_1(E)t_2(E) = \mathcal{O}(E^2) \quad \text{as } E \to 0.$$

□

Corollary 3.2. *Let $\Omega \subseteq \mathbb{R}^n$ be bounded and suppose that it satisfies an interior cone condition. Let $f : \Omega \longrightarrow \mathbb{R}_{\geq 0}$, $f \in L_2(\Omega)$, and let $\kappa \in C^{2k}(\Omega \times \Omega)$ be a strictly positive definite kernel so that $f \in \mathcal{N}_\kappa(\Omega)$. Moreover, let r be the κ-based interpolant of f at $\mathcal{X}$ as in (1). Therefore,*

$$\mathrm{cSSIM}(f, r) = \frac{1}{1 + \mathcal{O}(h^{2k})} \quad \text{as } h \to 0.$$

Proof. As observed in Remark 1, Theorem 2.1 yields $E_{f,r} = \mathcal{O}(h^k)$ as $h \to 0$, which implies $\mathcal{O}(E_{f,r}^2) = \mathcal{O}(h^{2k})$. □

We observe that the convergence rate in terms of the similarity index cSSIM is strongly related to the smoothness of the considered kernel, as a consequence of Theorem 2.1.
More specifically, while we showed that the convergence of the uniform error implies the convergence in the cSSIM index, we remark that the converse is not true. Indeed, for example, letting $\Omega = [-1,1]$, $\varepsilon > 0$,

$$f(x) = \begin{cases} \varepsilon & \text{if } x = 0, \\ 0 & \text{otherwise,} \end{cases} \qquad x \in \Omega,$$

and the sequence of functions $(f_n(x))_{n\in\mathbb{N}}$, where

$$f_n(x) = \begin{cases} \varepsilon & \text{if } x \in [-e^{-n}, e^{-n}], \\ 0 & \text{otherwise,} \end{cases} \qquad x \in \Omega,$$

we have $E_{f,f_n} = \varepsilon \ \forall n \in \mathbb{N}$, while $\text{cSSIM}(f, f_n)$ quickly approaches 1 as n gets larger.
In the next section, numerical tests confirm the presented results.

4 Numerics

Let $\Omega = [-1,1]^2$ and $\Xi = \{\boldsymbol{z}_1, \dots, \boldsymbol{z}_M\}$, $M \in \mathbb{N}$, be an equispaced evaluation grid with step $\zeta = 5 \cdot 10^{-3}$.
In what follows, we test the convergence rate in terms of cSSIM in RBF interpolation. Moreover, we compare it with the convergence in terms of the standard uniform norm.
As a discrete approximation of the cSSIM, we take the Matlab built-in implementation of the SSIM index, which coincides with the formulation in (4), with $c_1 = c_2 = 10^{-3}$. Concerning the uniform norm, we consider the Maximum Absolute Error (MAE) which is defined as

$$\text{MAE}(f, r) = \max_{1 \le i \le M} |f(\boldsymbol{z}_i) - r(\boldsymbol{z}_i)|.$$

For a better comparison with the MAE, we plot the dissimilarity DSSIM instead of the SSIM index.

In our tests, we consider the following strictly positive definite radial kernels

$$\begin{aligned} &\varphi_1^\varepsilon(r) = (1-\varepsilon r)_+^4(4\varepsilon r + 1), && \textit{Wendland } C^2, \\ &\varphi_2^\varepsilon(r) = e^{-\varepsilon r}\left(15 + 15\varepsilon r + 6\varepsilon^2 r^2 + \varepsilon^2 r^3\right), && \textit{Matérn } C^6, \end{aligned}$$

where $\varepsilon > 0$ is the so-called *shape parameter* and, with $\boldsymbol{x} = (x_1, x_2)$, the test functions $f_1, f_2 : \Omega \longrightarrow \mathbb{R}$ defined as

$$f_1(\boldsymbol{x}) = 2(x_1 x_2)^2 - \text{sinc}(x_1)\,\text{sinc}(x_2) + 1, \ f_2(\boldsymbol{x}) = e^{-(x_1+x_2)} - 3x_1 + x_2 + 5.$$

As interpolation sets, we take $\mathcal{X}_k$, $k = 1, \dots, 4$, so that $\mathcal{X}_k$ is an equispaced grid on Ω with step $\xi_k = 4 \cdot 2^{-(k-1)} 10^{-1}$ and, consequently, with fill distance $h_k = \sqrt{2}\xi_k/2$.

In Figure 1 and Figure 2, we fix $\varepsilon = 1$ and we display the convergence results in terms of the fill distances h_k, $k = 1, \dots, 4$. We adopt the notation

$$r_i^k[j] = r_{\varphi_i^1}^{\mathcal{X}_k}[f_j], \quad i, j = 1, 2, \ k = 1, \dots, 4,$$

for the kernel-based interpolant built on φ_i^1 which interpolates f_j at $\mathcal{X}_k$.

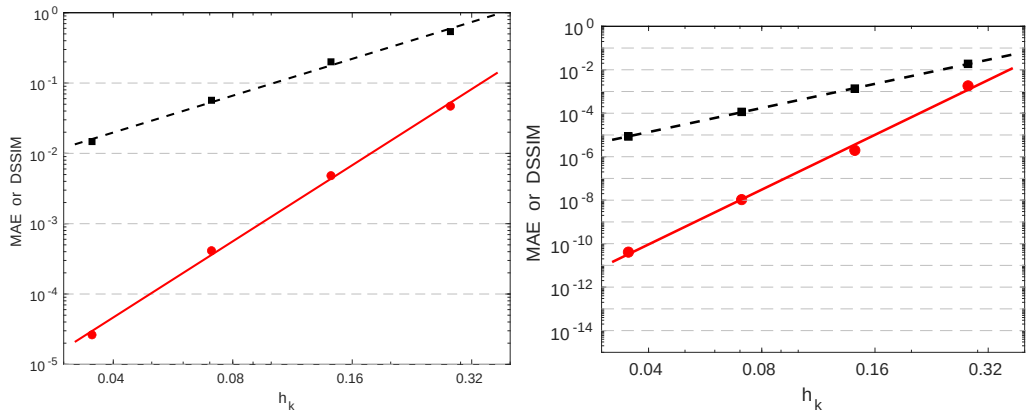

Figure 1: Convergence rates: $\left(h_k, \text{MAE}(f_1, r_i^k[1])\right)$ (black squares) and $\left(h_k, \text{DSSIM}(f_1, r_i^k[1])\right)$ (red circles) varying $k = 1, \dots, 4$. The case $i = 1$ is on the left, while the case $i = 2$ is on the right. The red and dashed black lines are the respective regression lines.

Then, in Table 1 we verify the results of Theorem 3.1. There, the reported experimental slopes refer to the regression lines in Figure 1 and Figure 2, while the theoretical slopes are derived from (3).
Finally, in Figure 3 and Figure 4 we fix the interpolation set $\mathcal{X}_k$ by setting $k = 3$ and we display the behaviour of the MAE and DSSIM indices varying the value of the shape parameter $\varepsilon \in [0.05, 2]$ of the kernels.

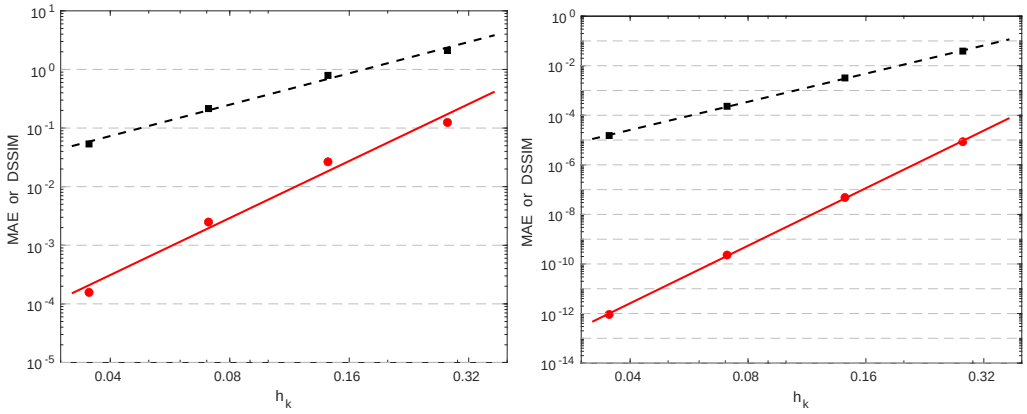

Figure 2: Convergence rates: $\left(h_k, \text{MAE}(f_2, r_i^k[2])\right)$ (black squares) and $\left(h_k, \text{DSSIM}(f_2, r_i^k[2])\right)$ (red circles) varying $k = 1, \ldots, 4$. The case $i = 1$ is on the left, while the case $i = 2$ is on the right. The red and dashed black lines are the respective regression lines.

Kernel	Theor. slopes		Exper. slopes f_1		Exper. slopes f_2	
	MAE	DSSIM	MAE	DSSIM	MAE	DSSIM
φ_1^1	1.5	3	1.74	3.60	1.78	3.23
φ_2^1	3.5	7	3.69	8.38	3.78	7.72

Table 1: The theoretical slopes concerning φ_1^1, φ_2^1 and the experimental slopes obtained in the interpolation of f_1 and f_2.

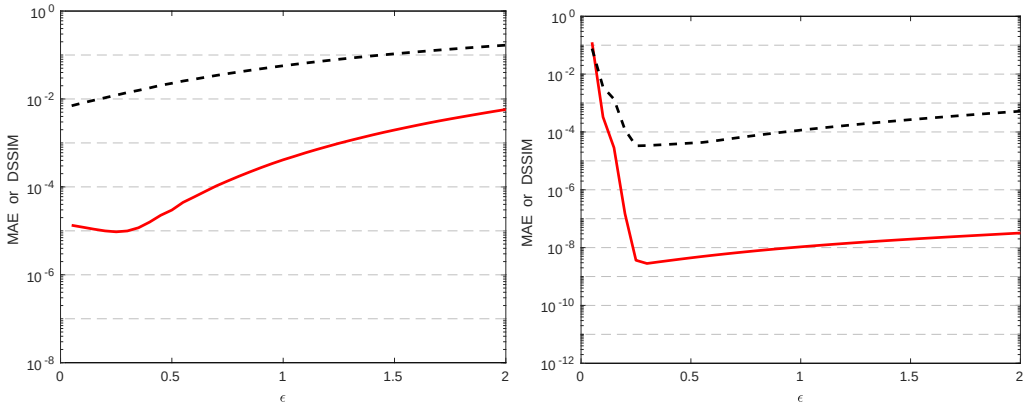

Figure 3: Interpolation of f_1 varying ϵ and taking φ_1^ε (left) and φ_2^ε (right): the MAE is displayed in dashed black, while the DSSIM index is in red.

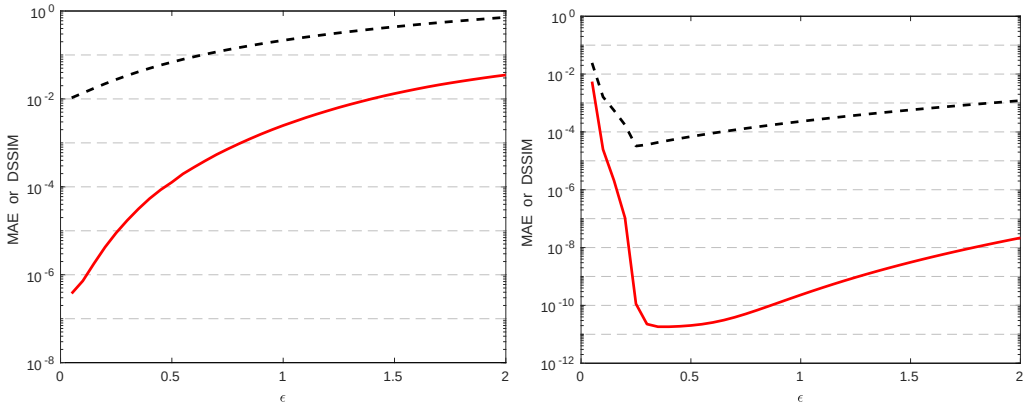

Figure 4: Interpolation of f_2 varying ϵ and taking φ_1^ε (left) and φ_2^ε (right): the MAE is displayed in dashed black, while the DSSIM index is in red.

5 Conclusions

In this paper, after introducing the cSSIM index as an extension of standard SSIM, we analysed the convergence behavior in terms of cSSIM in the framework of RBF interpolation. There, the role played by the regularity of the kernel is proved and then verified by means of numerical tests.

We point out that the carried out analysis may be also considered in other interpolation frameworks. Therefore, future work consists in investigating on the cSSIM index in different approximation settings, as well as in improving the presented results by looking for more refined bounds, especially in the case of irregular kernels.

Acknowledgements

This research has been accomplished within Rete ITaliana di Approssimazione (RITA), with the support of GNCS-INδAM and partially funded by the ASI - INAF grant "Artificial Intelligence for the analysis of solar FLARES data (AI-FLARES)".

References

[1] D. Brunet, J. Vass, E. R. Vrscay, Z. Wang. Geodesics of the Structural Similarity index. *Appl. Math. Lett.*, 25:1921–1925, 2012.

[2] D. Brunet, E. R. Vrscay, Z. Wang. On the Mathematical Properties of the Structural Similarity Index. *IEEE Transactions on Image Processing*, 21(4):1488–1499, 2012.

[3] S. De Marchi, W. Erb, F. Marchetti. Spectral filtering for the reduction of the Gibbs phenomenon for polynomial approximation methods on Lissajous curves with applications in MPI. *Dolomites Res. Notes Approx.*, 10:128–137, 2017.

[4] S. De Marchi, W. Erb, F. Marchetti, E. Perracchione, M. Rossini. Shape-Driven Interpolation with Discontinuous Kernels: Error Analysis, Edge Extraction and Applications in MPI. *SIAM J. Sci. Comput.*, 42(2):B472–B491, 2020.

[5] S. De Marchi, F. Marchetti, E. Perracchione. Jumping with Variably Scaled Discontinuous Kernels (VSDKs). *Bit Numer. Math.*, 60(2):441–463, 2020.

[6] G.E. Fasshauer. Meshfree Approximations Methods with MATLAB. *World Scientific*, Singapore, 2007.

[7] A. Rehman, K. Zeng, Z. Wang. Display Device-Adapted Video Quality-of-Experience Assessment. *Human Vision and Electronic Imaging XX, Proc. SPIE*,9394, 2015.

[8] M. P. Sampat, Z. Wang, S. Gupta, A. C. Bovik, M. K. Markey. Complex Wavelet Structural Similarity: A New Image Similarity Index. *IEEE Transactions on Image Processing*, 18(11):2385–2401, 2009.

[9] A. Sommariva, M. Vianello. Numerical Cubature on Scattered Data by Radial Basis Functions. *Computing*, 76:295–310, 2006.

[10] Z. Wang, A C. Bovik, H. R. Sheikh, E. P. Simoncelli. Image quality assessment: from error visibility to structural similarity. *IEEE Transactions on Image Processing*, 13(4):600–612, 2004.

[11] H. Wendland. Scattered Data Approximation. *Cambridge Monogr. Appl. Comput. Math.*, 17, Cambridge Univ. Press, Cambridge, 2005.

[12] H. Zhao, O. Gallo, I. Frosio, J. Kautz. Loss Functions for Image Restoration With Neural Networks. *IEEE Transactions on Computational Imaging*, 3(1):47–57, 2016.